Nanoscale

PAPER

View Article Online
View Journal | View Issue

Cite this: *Nanoscale*, 2015, **7**, 198

Large variations in both dark- and photoconductivity in nanosheet networks as nanomaterial is varied from MoS_2 to WTe_2†

Graeme Cunningham,[a] Damien Hanlon,[a] Niall McEvoy,[b] Georg S. Duesberg[b] and Jonathan N. Coleman*[a]

Received 26th August 2014,
Accepted 22nd October 2014

DOI: 10.1039/c4nr04951a

www.rsc.org/nanoscale

We have used solution processing techniques to fabricate thin-film networks of nanosheets of six different transition metal dichalcogenides; MoS_2, $MoSe_2$, $MoTe_2$, WS_2, WSe_2 and WTe_2. We have measured both the dark conductivity and the photoconductivity under broad band illumination in the intensity range from 0–1500 W m^{-2}. The dark conductivity varied from ~10^{-6} S m^{-1} for MoS_2 to ~1 S m^{-1} for WTe_2, with an apparent exponential dependence on bandgap. All materials studied show photocurrents which rise slowly with time and depend sub-linearly on light intensity, both hallmarks of trap limited processes. Because the photoresponse depends relatively weakly on bandgap, the ratio of photo- to dark conductivity is largest for the sulphides because of their lower dark conductivities. As such, MoS_2 and WS_2 may be best suited to photo-detection applications. However, due to their lower bandgap and superior conductivity, WSe_2 and WTe_2 might prove more effective in other applications, for example in photovoltaic cells.

Introduction

The study of 2-dimensional (2D) materials is becoming one of the most exciting areas of nanoscience. There are many families of 2D materials, all displaying different properties and each with its own set of strengths and weaknesses.[1–5] One of the most well-known classes of inorganic 2D material are the transition metal dichalcogenides (TMDs), characterised by the chemical formula MX_2. Here M is a transition metal atom (usually Mo or W) and X a chalcogen (S, Se or Te). Probably the most heavily studied TMDs are MoS_2 and WS_2, although dozens of these materials exist.[6,7] Depending on the combination of metal and chalcogen atoms these materials can be insulators, semiconductors or metals. They crystallise with hexagonal symmetry in a covalently bonded structure to form 2D monolayers which stack together to form 3D crystals.[8] Adjacent layers are bound by weak van der Waals interactions, allowing exfoliation of bulk crystals into mono and few layer nanosheets.[9] The electronic properties vary among TMDs; for example as the mass of the chalcogen atom increases (*i.e.* from S to Se to Te), the bandgap decreases. For a given TMD, the band structure depends sensitively on the layer number.[10–20] As such, these materials have generated a huge amount of interest due to the possibility of using them in electronic or optoelectronic applications.[7]

For most researchers, exploiting the electronic properties of TMDs (and other 2D materials) involves the study of very high quality monolayer nanosheets, deposited on substrates either by micromechanical cleavage[21] or growth.[22,23] This approach has resulted in the demonstration of a host of high-performance devices such as transistors,[21] photodetectors,[24,25] logic circuits[26] and solar cells.[27,28] However, we believe another approach may be useful and should not be neglected. Once suspended in liquids,[29] nanosheets can be cheaply and easily deposited to form networks which may be useful in an array of applications. Already, such networks are becoming important in electrochemical applications such as battery[30,31] or supercapacitor electrodes[32,33] or as catalysts.[34–36] However, these networks may also have applications in printed electronics.[37–40] In such applications, the main limitation will be that the carrier mobility in a network would be expected to be much smaller than that in an individual nanosheet because of the necessity of inter-sheet hopping. However, in networks of nanotubes[41] and graphene nanosheets[42], the ratio of nano-object to network mobilities is often as low as 100. As TMD nanosheets have mobilities of ~100 cm^2 V^{-1} s^{-1},[21] we might hope to develop networks of nanosheets with mobilities of

[a]*School of Physics, CRANN and AMBER Research Centres, Trinity College Dublin, University of Dublin, Dublin 2, Ireland*
[b]*School of Chemistry, CRANN and AMBER Research Centres, Trinity College Dublin, University of Dublin, Dublin 2, Ireland. E-mail: colemaj@tcd.ie*
†Electronic supplementary information (ESI) available: See DOI: 10.1039/c4nr04951a

~1 cm^2 V^{-1} s^{-1}, competitive with printable organics.[43] Thus, we believe it is important to take the first steps toward using such networks in (opto)electronic applications.

In order to develop printed electronics applications of 2D materials, appropriate methods to disperse high quality nanosheets in liquids are required. Liquid phase exfoliation is a solution processing method, capable of generating industrial quantities[44] of exfoliated 2D nanosheets dispersed in organic solvents[45,46] or aqueous surfactant solutions.[46,47] The dispersed nanosheets are of extremely high quality and can be sorted by size and thickness.[47] Such dispersions are extremely processable, can be formed into films or coatings, or can be mixed with other systems to produce composites.[29] We can envisage utilising high throughput, low temperature processing (roll-to-roll, dip-coating, spraying or inkjet printing) to produce functional structures from these exfoliated nanosheets. Combining different types of nanomaterials will allow the production of a wide range of devices from these dispersions.[38,39,48,49]

Group VI (Mo or W) TMDs are nominally semiconducting with optical bandgaps of ~1.8 eV, 1.5 eV and 1.1 eV for the sulphides, selenides and tellurides respectively and indirect bandgaps ranging from ~1.3 to ~0.9 eV.[6,7] MoS_2 and WS_2 are known to exhibit photoconductivity in their mono and few layer forms.[23–25,50–55] Being abundant, cheap, non-toxic, flexible[56,57] and photo-stable[58] with extremely high absorption coefficients[59] and the absence of dangling bonds,[60] these materials are ideal candidates for a range of applications such as high quality solar cell absorbing layers. As such, we believe photoconductivity is an excellent starting point for the demonstration of optoelectronic capability of networks of liquid exfoliated nanosheets. Indeed, we, and others,[48] have already demonstrated photoconductivity from both solution cast[37] and inkjet printed[38] networks of MoS_2. However thus far, the photoconductivity of other group VI MSe_2 and MTe_2 based TMDs has not been studied in mechanically-cleaved, CVD-grown or solution-cast forms. This is unfortunate as, due to their narrower bandgaps, these materials would extend the spectral range of any device whose operation requires optical absorption.

Here we report the first comparative study of both dark- and photoconductivity of solution processed films of MoS_2, $MoSe_2$, $MoTe_2$, WS_2, WSe_2 and WTe_2 nanosheets. The photocurrent response of these materials to a range of light intensities from a broadband source has been investigated as a function of time and intensity. We find significant differences in performance which mainly stem from the broad range of dark conductivities in these materials.

Results & discussion

In this paper we use liquid-based techniques to exfoliate layered crystals of TMDs into suspensions of nanosheets which can then be formed into thin films. The aim of this work is to compare the photoconductive properties of such films for a range of TMDs, namely MoS_2, $MoSe_2$, $MoTe_2$, WS_2, WSe_2 and WTe_2. When prepared in this way, such films consist of disordered networks of exfoliated nanosheets.[46] In general, solution processing tends to give nanosheets with a range of sizes and thicknesses.[47] The bandgap of all TMDs tends to vary strongly with nanosheet thickness – for example while monolayer MoS_2 has a direct bandgap of 1.8 eV, thicker nanosheets (*e.g.* bilayers, trilayers *etc.*) have lower indirect bandgaps. Above ~6 layers, the indirect band gap approaches that of a bulk crystal (~1.2 eV for MoS_2). This is a problem for a study such as this one because a film of as-prepared nanosheets will contain platelets of all thicknesses from 1 to >10 monolayers. This will render the electronic properties of the network both spatially inhomogeneous and ill-defined, making comparisons between materials difficult. As suggested previously,[39] we propose to address this issue by removing all thin nanosheets from the dispersion before film formation. This will result in thin films consisting predominately of nanosheets with >10 layers, all of which have bandgaps close to the bulk value.

To do this, we used a centrifugation-based size selection method to remove all small thin nanosheets (see Methods). TEM analysis showed the resulting material to consist of electron-opaque, micron sized nano-platelets (Fig. 1A–F). The opacity of these objects confirms them to be much thicker than are found using normal liquid exfoliation (*i.e.* without size selection).[46,47] The mean nanosheet length varied from 1.4 to 0.6 μm depending on the TMD type (*e.g.* depending on its density, see ESI†).[37] However, even though these nanoplatelets are relatively large, most importantly, they are still solution processable.

We used these size-selected nanosheet dispersions to prepare thin films from each of the six nanosheet types. We used a variation of the Langmuir–Blodgett method as described in our previous work.[37] The as-formed films were estimated to be roughly 1 μm thick from the mass of each material deposited onto the water surface. In all cases, they were opaque and appeared uniform to the naked eye. SEM examination (Zeiss Ultra Plus) showed continuous films when viewed at large length scales (>10 μm) (Fig. 1G). However, when viewed at higher magnification, films are confirmed to be composed of a disordered array of TMD flakes (Fig. 1H). Raman spectra were recorded using an excitation wavelength of 532 nm for both starting powders and films of all materials (see ESI†). Peak positions coincide well with literature values for bulk TMDs,[15,61,62] with slight shifts as is sometimes the case for powdered samples.[37,63]

In this study we fabricate simple two terminal devices by depositing TMD films onto pre-patterned gold electrodes as shown in Fig. 1J. This was carried out for all six TMDs. These devices had channel length and width of L = 50 μm and w = 1 cm respectively. This channel length is much larger than even the maximum nanosheet size meaning that inter-flake charge transfer will play an important role in the electrical properties.

We opted to use gold electrodes for films of all six TMDs. It has been suggested that Gold can form quasi-Ohmic contacts

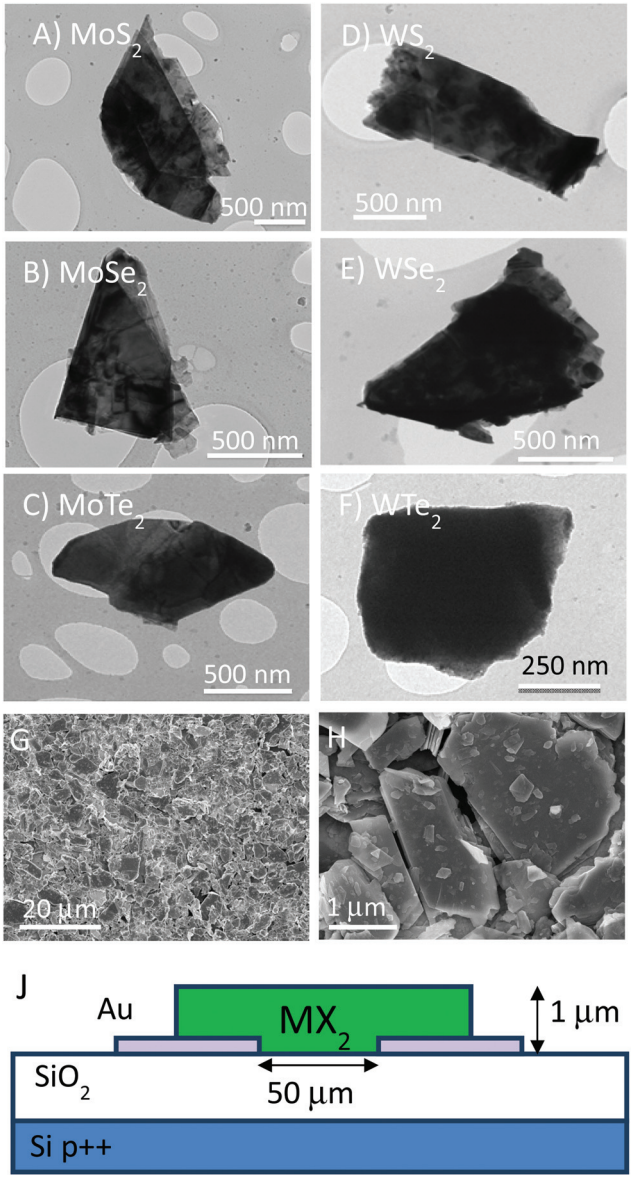

Fig. 1 (A–F) TEM images of nanoplatelets of (A) MoS_2, (B) $MoSe_2$, (C) $MoTe_2$, (D) WS_2. (E) WSe_2 and (F) WTe_2. (G) SEM image of typical MoS_2 film with magnified view shown in H. (J) Schematic of the device arrangement used in this work.

to MoS_2 monolayers[21,26,64] at room temperature.[65,66] This is in contrast to what would be expected from standard band alignment arguments,[67,68] a contradiction that has been attributed to factors such as Fermi level pinning close to the CB.[66,69–71] While a finite barrier has been reported when using Au to contact thicker MoS_2 [27,52,53,55,72] and WS_2 [28,73] samples, it is often lower than that expected for a typical metal-semiconductor junction.[28,65,66] Several studies on the electrical properties of WSe_2 have been published recently.[74–77] This material is less prone to Fermi level pinning than MoS_2 and can operate in both[76] p-type[75] or n-type[74] mode depending on the contact metal selected. Much less work has so far been published on electrical characterisation of $MoSe_2$,[78,79] $MoTe_2$ [80] and WTe_2, making electrode choice difficult. In addition, the effect of the interaction of metal atoms with the nanosheet edges is not known and may contribute to unexpected interfacial effects. Our decision to use gold on all six materials was based on a desire for consistency coupled with data from preliminary experiments which showed all materials to give symmetric *I–V* curves when using gold electrodes. However, we accept that future studies might find other metals more appropriate for achieving injecting contacts to these materials.

Shown in Fig. 2A–F are *I–V* curves taken for each material in the dark (black lines). These are plotted together for comparison in Fig. 2G. As indicated above, the curves are symmetric about the origin in all cases. The dark conductivities (as deter-

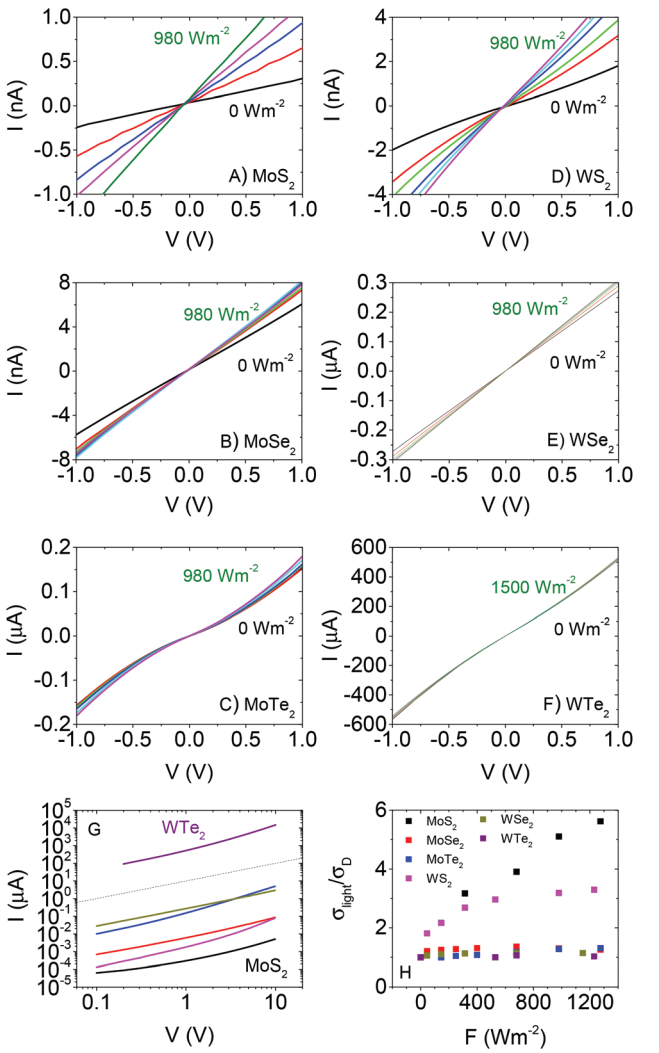

Fig. 2 Dark and illuminated current–voltage curves measured for thin films of (A) MoS_2, (B) $MoSe_2$ (C) $MoTe_2$, (D) WS_2, (E) WSe_2 and (F) WTe_2. The incident intensity varied from ~50 to 980 W m^{-2} with the exception of WTe_2, where it was varied up to 1500 W m^{-2}. N.B. The current scales in A, B and D are nA while in C, E and F they are µA. (G) Dark *I–V* curves for each material. The dashed line represents linearity. (H) Ratio of conductivity under illumination to dark conductivity, plotted *versus* incident intensity, for all six materials. N.B The colour scheme in G is the same as that in H.

mined from the slope of the curve around the origin) varied strongly over the material set from ~10^{-6} S m^{-1} for MoS_2 to ~1 S m^{-1} for WTe_2. This variation will be discussed in more detail below. In all cases, the curves were super-linear at higher voltages. It should be noted that this is not an automatic signature of non-Ohmic contacts but can be caused by space charge effects.[81] The data for MoS_2 is similar to previous data for in-plane conductivity in solution processed films.[82] However, it is ~3 orders of magnitude higher than that found for out of plane measurements on similarly prepared films,[37] consistent with conductivity anisotropies in layered materials such as graphite. The variation in conductivity among the materials will be discussed below.

To compare the photoconductivity of the different TMDs we study the effect of illuminating each sample with a broad-band light source. A solar simulator (Newport 960000), fitted with a Xe arc discharge lamp (150 W) and air mass (AM) 1.5 filter was used. The lamp was calibrated against a standard Si based reference cell. Light intensity at the sample was varied using a set of neutral density filters (NDFs) from Newport. *I–V* curves for each material measured at different light intensities are shown in Fig. 2A–F. All curves remain symmetric about the origin with linear, followed by supralinear regions as observed for the dark current. In addition, clear increases in current with light intensity are observable. For all data sets, we calculate the conductivity from the slope of the *I–V* curve close to the origin: $\sigma = (L/wt)(dI/dV)_{V=0}$. We note that this parameter only strictly represents the conductivity in the case of Ohmic contacts. The ratio of conductivity under illumination to dark conductivity (σ_{light}/σ_D) is plotted *versus* light intensity in Fig. 2H. It is clear from this data that the relative photoconductive effect is strongest in MoS_2, followed by WS_2 with the other materials showing comparatively weak effects.

It is also worth noting that, for each material, the voltage range over which the *I–V* curves display linearity broadens slightly as a function of light intensity. This is a common effect in polycrystalline semiconductor films and is associated with a slight lowering of potential barriers present at the inter-flake junctions due to the presence of photo-generated carriers.[83–87] This will manifest itself as a small increase in carrier mobility with light intensity.

The time dependence of the photoresponse was characterised for each material by opening and closing a shutter between lamp and sample while increasing the intensity each time shutter was closed. Typical examples of current-time traces are shown in Fig. 3A–F. For all light intensities, on illumination the photocurrent exhibits a fast increase followed by a slow increase to steady state (SS) as observed previously for out of plane measurements on MoS_2 films.[37] The same pattern for the decay is followed in the opposite order once illumination is ceased. The fast components are associated with the initial equilibration of the carrier generation and recombination rates.[67] The slow components are due to trap filling and emptying on rise and decay respectively.[67] A slow photoresponse such as that observed here is expected in films with a large density of trap states.[67] In most cases (see Fig. 3G for example and ESI† for complete data sets), the time constants associated with the slow rise and decay of photocurrent fall off with intensity as expected for systems with a distribution of localised states. Such behaviour is consistent with an increased number of such states acting as recombination centres at higher intensities once illumination has ceased.[67,88] However, we note that the data is much more scattered than that previously observed for out of plane, solution processed MoS_2 photodetectors.[37] The time constants, measured for a rising photocurrent in each material at a fixed intensity of F = 250 Wm^{-2}, are given in Fig. 3H and are typically tens of seconds. Interestingly, there seems to be a pattern whereby the time constants scale with material as MS_2 > MTe_2 > MSe_2 for both Mo- and W-based systems. This may suggest that the trap density depends on the chalcogen.[67] Strangely, the MoS_2 time constant

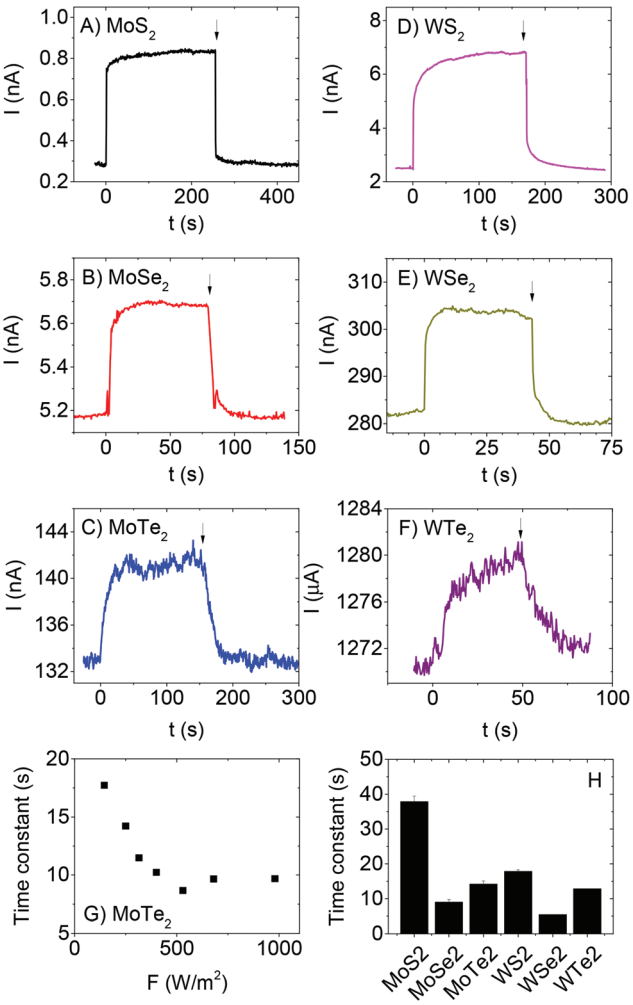

Fig. 3 Current *v* time graphs for (A) MoS_2, (B) $MoSe_2$ (C) $MoTe_2$, (D) WS_2, (E) WSe_2 and (F) WTe_2. In all cases, V = 1 V and the light was turned on at t = 0 s (F = 250 W m^{-2}) and turned off at the time indicated by the arrow. Note that in all cases, approximately exponential rises and decays of photocurrent were observed. (G) Time constant measured for rise of $MoTe_2$ photocurrent, plotted *versus* incident intensity. (H) Average time constants associated with the photocurrent rise, measured at F = 250 W m^{-2}, for each material.

is lower than that observed from out of plane photocurrent measurements (~100 s).[37] In any case, this data shows the photoresponse to be trap-limited for all six materials.[67]

We measured the steady state photocurrent, ΔI_{SS}, (V = 1 V) as a function of light intensity for all six materials. We then converted this to photoconductivity (defined as $\sigma_{PC} = \sigma_{light} - \sigma_D$) using $\sigma_{PC} = \Delta I_{SS} L/(wtV)$ where L is the electrode spacing (50 μm), w is the electrode length (1 cm), t is the electrode thickness (1 μm) and V is the applied voltage (1 V). This data is plotted in Fig. 4A–F. The first thing to note is there is significant variation of the photoconductivity at high intensity (*i.e.* that at 980 W m^{-2}). As shown in Fig. 4G, this varies from <10 μS m^{-1} for MoS_2 to >50 mS m^{-1} for WTe_2. For each material, a sublinear dependence of photoconductivity on light intensity was observed, in agreement with previous measurements on films of liquid exfoliated MoS_2 nanosheets.[37] This behaviour is consistent with a number of reports[89–91] on materials containing broad trap distributions, which all show power-law behaviour, usually expressed as

$$\sigma_{PC} = KF^{\gamma} \quad (1)$$

where K and γ are material constants. Large values of both constants lead to large photocurrents. Such behaviour is consistent with a simple model by Rose[67,88] for materials with exponential trap distributions which we will discuss below. Fitting the data showed K to vary over ~2 orders of magnitude (see below), with values of γ ranging from 0.38 (WS_2) to 0.84 (WTe_2). This is reasonably consistent with Rose's model which predicts that $0.5 \leq \gamma \leq 1$ for systems with broad trap distributions within the bandgap.[88]

We plot the fit curves together in Fig. 4H for comparison. It is clear from this panel that, over most of the measured intensity range, the photoconductivity tends to scale as WTe_2 > WSe_2 > $MoTe_2$ > WS_2 > $MoSe_2$ ~ MoS_2. Clearly, W-based materials are superior to Mo-based ones while performance also appears to depend on bandgap (MTe_2 > MSe_2 > MS_2).

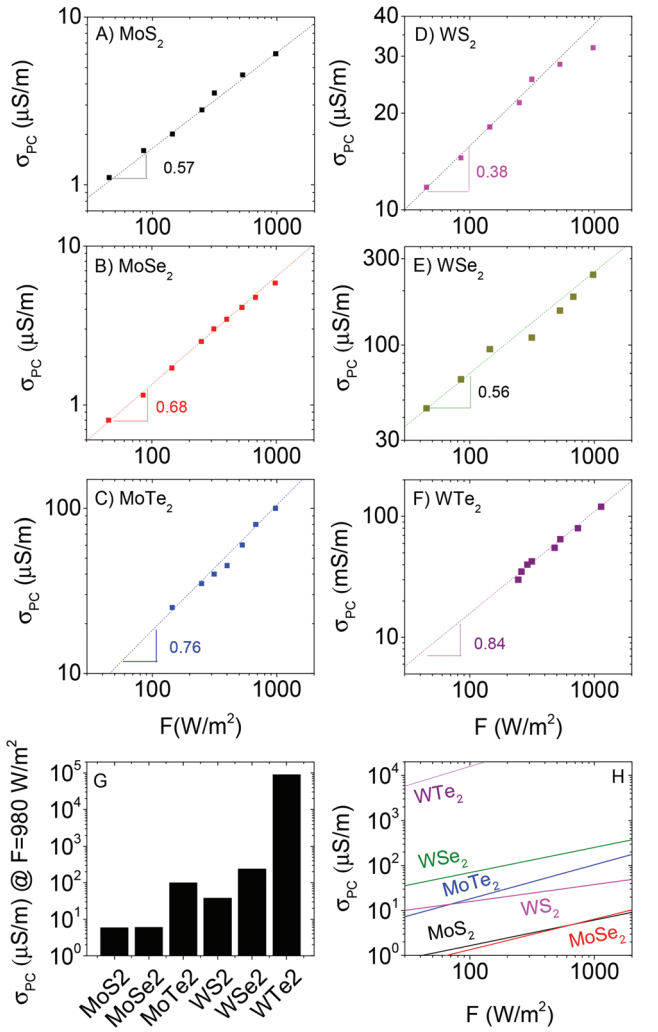

Fig. 4 Steady state photoconductivity plotted *versus* light intensity for (A) MoS_2, (B) $MoSe_2$ (C) $MoTe_2$, (D) WS_2, (E) WSe_2 and (F) WTe_2. In all cases, the photoconductivity was measured at V = 1 V. (G) Photoconductivity for each material, measured at 980 W m^{-2}. (F) The fit curves have been plotted together to allow comparison between materials.

Discussion

The data above clearly demonstrates trap-limited photoconductivity for all six TMDs studied. Fig. 2 and 4 show photoconductive behaviour which varies significantly from material to material. It would be of great interest to begin to develop an understanding as to the nature of these differences. The most basic physical parameter which varies across this material set is the bandgap. Because we have deliberately chosen to study relatively thick nanosheets, the appropriate bandgap is the bulk, indirect bandgap which varies from ~1 eV for the tellurides to ~1.2–1.3 eV for the sulphides (see ESI† for more information). Whilst the narrower bandgap for the tellurides obviously ensures absorption of a greater percentage of the broadband light, this will not be the only mechanism affecting the photoconductive response.

Shown in Fig. 5A is the dark conductivity plotted as a function of bulk (indirect) bandgap for all six materials studied. The open symbols represent the mean values averaged over a number of different samples while the closed symbols represent the data collected from the samples for which the photoconductivity data was presented above. The conductivities range over 6 orders of magnitude, from ~10^{-6} S m^{-1} for MoS_2 to >1 S m^{-1} for WTe_2. We note that the conductivity value for WTe_2 is very large, a fact that may be useful for a range of applications. This graph shows a clear trend, with dark conductivity falling with increasing bandgap for both Mo- and W-based TMDs. Interestingly, the data for both material types are consistent with $\sigma_D \propto e^{-E_g/1.5kT}$ (dashed lines). This is reminiscent of the behaviour expected for intrinsic semiconductors (*i.e.* with Fermi energy close to the centre of the gap), where the conductivity is given by

$$\sigma_D = \mu e N_c e^{-E_g/2kT} \quad (2)$$

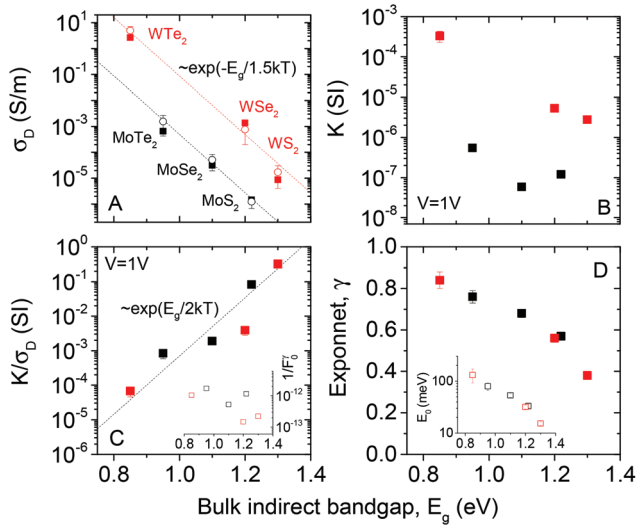

Fig. 5 Bandgap dependence of photo-conductive parameters. (A) Dark conductivity, (B) *K*-parameter (eqn (1)), (C) ratio of *K* parameter to dark conductivity and (D) intensity exponent plotted *versus* bulk, indirect bandgap. The inset in (C) plots $1/F_0^{\gamma}$ while that in (D) shows the characteristic trap energy as a function of bulk, indirect bandgap. In (A), the dashed lines represent $\sigma_D \propto \exp(-E_g/1.5kT)$, the open symbols represent the mean over ~5 independent samples, while the close circles represent the samples used for the presented photoconductivity measurements. In (C), the dashed line represents $\sigma_D \propto \exp(E_g/2kT)$.

where the thermally activated carrier density, n (or p), is given by $n = N_c e^{-E_g/2kT}$. Here μ is the electron (hole) mobility, N_c is the effective number of states per volume in the conduction (valence) band and E_g is the energy gap. In eqn (2), the $E_g/2$ component reflects the distance from Fermi energy to the band edge, which is of course $E_g/2$ for an intrinsic semiconductor. For a doped semiconductor, $E_g/2$ can be replaced by E_g/a, where $a > 2$.

The fact that the experimental slopes in Fig. 5A are $-1/1.5kT$, rather than $-1/2kT$ is interesting. It implies that eqn (2) cannot explain all of the bandgap dependence. Assuming Ohmic contacts, this in turn suggests that the mobility depends on bandgap roughly as $\mu = \mu_0 e^{-E_g/bkT}$, where b is a constant. Such an exponential dependence can be rationalised by the fact that the mobility is limited by inter-sheet hopping which will depend on both band-structure and temperature. Then, we can express the dark conductivity of the materials under study here as

$$\sigma_D = e\mu_0 e^{-E_g/bkT} N_c e^{-E_g/akT} = e\mu_0 N_c e^{-(1/a+1/b)E_g/kT} \quad (3)$$

where empirically, $(1/a + 1/b) = 1/1.5$. Below, we will attempt to ascertain the values of a and b. However, it must be noted that, were the current limited by the presence of Schottky barriers, an exponential dependence of current on bandgap might conceivably be observed (see ESI†). As mentioned elsewhere in this paper, more work is required to fully understand the transport properties of these materials.

We now turn to the photoconductivity. From the fits in Fig. 5, we can plot the parameter *K versus* bulk indirect bandgap in Fig. 5B. This clearly shows the WX_2 compounds to display *K*-values which are 10–100 times larger than those of the MoX_2 systems. Sublinear power-law dependence of photoconductivity on intensity such as observed here has been treated in a simple model by Rose.[67,88] He considered materials with a broad trap distribution which decays exponentially from the band edge as $e^{-\Delta E/E0}$ where ΔE is the energy relative to the band edge and E_0 is the characteristic trap energy. In this case Rose derived an equation for the photo-induced carrier density, n_{PC}, which can be expressed as

$$n_{PC} = N_c \left[\frac{f}{N_T \nu S N_c}\right]^{E_0/(kT+E_0)} \quad (4)$$

where N_c is the effective density of states in the conduction band, f is the electron–hole pair generation rate (s^{-1} m^{-3}), N_T is the total trap density (m^{-3}), ν is the thermal velocity of carriers, S is the recombination cross-section and E_0 is the representative trap energy (difference from the band-edge). Assuming the films are thick enough to absorb all incident light in the resonant regime (which we approximate as photon energies larger than the direct bandgap of the material), then f is related to the total incident intensity F by $f = cF$ where c is related to the fraction of incident light absorbed: $c = \int_{\nu=E_{g,direct}/h}^{\nu=\infty} (I(\nu)/h\nu)d\nu / \int_{\nu=0}^{\nu=\infty} I(\nu)d\nu$ where $I(\nu)$ is the incident intensity in the range between ν and $\nu + d\nu$. We note that c is not expected to vary dramatically between materials. Assuming a solar spectrum, c falls from 0.4 to 0.15 as the direct bandgap is increased from 1.1 to 1.9 eV. With this in mind, we can rewrite eqn (1) in the form

$$\sigma_{PC} = KF^{\gamma} = \mu e N_c \left[\frac{F}{F_0}\right]^{\gamma} \quad (5)$$

where $F_0 = N_T \nu S N_c / c$ and $\gamma = E_0/(kT + E_0)$, and so the material properties are now contained in F_0 and γ. Then $K = \mu e N_c / F_0^{\gamma}$, suggesting the difference in *K*-values between WX_2 and MoX_2 compounds is due to differences in either μ or the trap related properties described by F_0^{γ}.

In order to separate the effects of mobility from trapping we consider the ratio of *K* and σ_D. Then, combining eqn (3) and (5):

$$\frac{K}{\sigma_D} = \frac{e^{E_g/akT}}{F_0^{\gamma}} \quad (6)$$

Values of K/σ_D are plotted *versus* (indirect) bandgap in Fig. 5C and show a clear exponential scaling with bandgap with data for all materials following the same trend. Assuming F_0^{γ} to be roughly invariant with bandgap (see below), fitting (dashed line) shows this behaviour to be consistent with $a = 2.33 \pm 0.45$. This is an interesting and rather surprising result, because, as described above, a value of $a = 2$ implies the materials to act as intrinsic semiconductors. Incidentally, that $a = 2$, allows us to use $(1/a + 1/b) = 1/1.5$ to find that $b = 6$. Approximating $a = 2$, we can use eqn (6) to calculate F_0^{γ}, finding values which are similar for all six materials: varying

from 6×10^{11} for $MoTe_2$ to 7×10^{12} for WSe_2 (in SI units). As mentioned above, the trap-related material properties are contained in F_0^{γ}, with small values of this parameter required for effective photoconductivity. Thus we can think of $1/F_0^{\gamma}$ as a figure of merit for photoconductivity. This is plotted in Fig. 5C (inset) and shows little variation between materials. We note that the data shown in Fig. 5C clearly shows that the material to material variations in both σ_D and K observed in Fig. 5A and B are mainly due to mobility and bandgap differences between compounds rather than strong variations in F_0^{γ}.

However, this data also highlights the limitations in Rose's model. Because the values of F_0^{γ} vary only weakly between materials, the variations in γ described above imply F_0 to vary over ~12 orders of magnitude among the materials studied. This is not realistic, meaning that while Rose captured the over-all behaviour with his model, the details are not correct.

The suggestion that these materials are close to intrinsic semiconductors is rather surprising as many papers have demonstrated that TMDs tend to be doped, resulting in Fermi energies close to the conduction band edge. Much of what is known about TMD doping generally comes from computational studies on MoS_2.[92,93] Many papers have shown that few and monolayer MoS_2 samples tend to be unintentionally n-doped.[21,65,94–98] Intrinsic defects such as stoichiometric deficiencies in compound semiconductors contribute localised states within the gap which can act as dopants depending on their energy.[99,100] Sulfur vacancies have a low formation energy in MoS_2 [69,70] and are thought to contribute a level close to the CB of monolayer MoS_2. This type of defect is known to be easier to produce and reside in higher concentration at flake edges than in the basal plane[70] and has been suggested as the source of the Fermi level pinning close to the CB.[11,71] However some reports also exist throughout the literature which show p-type operation from MoS_2.[101,102] This has been expanded on recently by studying locally resolved electrical characteristics of an MoS_2 sample.[66] This shows areas of high n- and p-type inducing defect densities on typical samples. Thus the conductivity of MoS_2 seems to depend on the experimental details in a non-trivial way. This aligns with older studies on bulk MoS_2 which commonly showed both n-[103] and p-type[104] operation. Much less is known about doping in other TMDs.

However, liquid exfoliated nanosheets are not particularly clean, tending to have non-negligible quantities of adsorbed residual solvent that is very hard to remove.[44] It is entirely possible that such adsorbed impurities tend to dope the nanosheets, bringing the Fermi energy toward the centre of the gap. Our method's use of organic solvents may induce effects not seen elsewhere in the literature. Indeed NMP has a high boiling point and is notoriously difficult to remove completely. In addition our disordered films have a large density of film edges. This influences the film doping *via* the localised states they produce. We may well have a scenario whereby the semiconductors here contain both donor (N_d) and acceptor (N_a) dopant species, resulting in a compensated semiconductor. The polarity of the conductivity is then governed by N_d–N_a with intrinsic behaviour expected if $N_d \approx N_a$.[105,106] However, in any case, were these materials actually intrinsic semiconductors, it is hard to see how gold could form quasi-Ohmic contacts with all of them. Thus, it is clear that more work is needed in this area.

This data clearly shows that the relatively poor photoresponse (represented here by σ_{light}/σ_D) for $MoSe_2$, WSe_2, $MoTe_2$ and WTe_2 (Fig. 2H) results from the large dark conductivities associated with these materials (Fig. 5A). Relative to the dark case, at 980 W m^{-2} the conductivity rises by a factor of 5 in the case of MoS_2 (best material) and a factor of 1.07 in the case of WTe_2 (worst). High dark currents are especially undesirable in photo-detection. This facilitates choice of a high bandgap material or insulators, to limit background of thermal carriers for practical applications. In addition to affecting the lowest measureable illumination high dark current also decreases sensitivity at low light levels.[107,108] This can be seen explicitly in Fig. 2H where the lowest light intensities used produced virtually no measureable signal in the case of $MoTe_2$ and WTe_2. Thus, the dark conductivities of most of the TMDs studied here are too high for photo-detection capabilities, especially when used with in-plane geometry.[109]

Shown in Fig. 5D is data for γ plotted *versus* the indirect bandgap for all six materials. This clearly shows a falloff in γ as the bandgap increases from 0.84 for WTe_2 to 0.38 for WS_2. While sublinear intensity dependence has been observed for a number of materials,[89–91] it is not usually observed for TMDs. This is because recent photoconductive studies of TMDs have been dominated by measurements on individual nanosheets of mono or few layer MS_2 samples. Most of these report linear dependence[23,50,53] of photocurrent on light intensity with only a minority reporting sub-linear[24,51] behaviour with γ values between 0.5[54] and 0.71.[52] In these cases, the sub-linear dependence is attributed to the presence of traps associated with the surface of the flakes. Liquid exfoliated nanosheets contain many flake edges which contribute localised states within the bandgap. Whether these states act as traps or recombination centres depends on the level of light intensity. As F increases, more trap states for electrons are converted into recombination centres, decreasing the majority carrier lifetime.[67,88] Therefore it is common for disordered semiconducting films to display diminished responsivity at high light intensities and so values of $\gamma < 1$.[90]

Rose's model links the exponent, γ, to the characteristic trap energy, E_0, as described above. We have used our data to calculate E_0 for each material (Fig. 5D inset). This data suggests the trap energy to fall off exponentially with bandgap, indicating the wider-gap materials to have shallower traps. The reason for this is not currently understood. However, we suggest that more detailed experimental work, or indeed computer modelling, is needed to understand in more detail the trap states in these materials. This will be critical if disordered networks of nanosheets are to be used in future (opto)electronic applications.

It is important to note that we see the results described here as being early stage research rather than being definitive. There are a number of factors which could affect both the

dark- and photoconductivity which we have not been considered in great detail. Firstly, we note that the mean nanosheet length varies considerably from 0.6 μm for WSe_2 to 1.4 μm for $MoSe_2$. We expect networks of larger platelets to show higher conductivity as few inter-platelet hops are required. However, as shown in the ESI,† the dark conductivity does not increase with nanosheet length. In addition, by using gold contacts for all devices, we may have electrode effects which vary from material to material. While we have assumed quasi-Ohmic contacts, we cannot rule out the possibility that the dark conductivities are limited by Schottky barrier effects. However, this would imply that the materials are even more conductive than reported in Fig. 5A. This would be surprising, especially for the more conductive of the six TMDs. In addition, we note that not much is known about contact effects when the metal electrode contacts to flake edges as well as the basal plane. Moreover, we do not know the doping level and so the Fermi energy in any of these materials. While we note that these materials appear to act, in some ways, like intrinsic semiconductors, this is unlikely to reflect the true nature of the materials. In a related point, we have noted that both MoX_2 and WX_2 materials behave like intrinsic semiconductors with mobilities and thermally activated carrier densities which depend on the bandgap. Obviously, it would be far better to measure both the mobility and carrier density for each material and analyse each individually, although such a study is beyond the scope of this paper. Nevertheless, we believe this work shows clear differences between the dark and electrical properties of the six TMDs under study. However, a considerable amount of future work is required before these differences are fully understood.

Conclusion

In summary, we have performed photoconductivity measurements on thin films, prepared from disordered networks of nanosheets of six transition metal chalcogenides. We find significant differences in performance, with both dark- and photo-conductivity varying widely between materials. The dark conductivity falls exponentially with bandgap with clear differences between Mo- and W-based materials. The photoconductivity could also be clearly differentiated between Mo- and W-based materials. Both the time- and intensity-dependence of the photoconductivity indicate the photoresponse to be limited by the presence of traps. The practical disadvantages of this are a slow photoresponse and a sublinear dependence of photoconductivity on intensity. Because of the dependence of dark conductivity on bandgap, the ratio of photo- to dark conductivity is much larger for the wide bandgap TMDs (MoS_2 and WS_2) even though they tend to display relatively small photoconductivities. Thus, this palette of materials presents different options, dependent on whether high absolute or relative photocurrent is required. For example, WSe_2, WTe_2 and $MoTe_2$ might prove more effective solar cell absorbing materials due to their lower bandgap and superior conductivity.

We note that the production of solution-processed films of inorganic nanosheets is still in its infancy. One could imagine many ways to improve these systems. For example, in the future we expect to develop much greater control over the size and thickness of nanosheets, leading to much more uniform networks. In addition, the development of better film formation techniques, whether by spray-, inkjet- or blade coating will lead to more controllable film morphologies. Moreover, chemistries might be developed to modify or eliminate the effect of traps, perhaps by healing chalcogen vacancies or pacifying edge states.[110] We see the current work as part of the early stages of development of (opto)electronic applications of solution processed nanosheet networks. However, we believe this field has much promise and will play an important role on the development of nanostructured printed electronics.

Methods

All materials were >99% pure and purchased in powder form. For each material supplier and particle sizes were as follows: MoS_2 (Sigma Aldrich, <2 μm), $MoSe_2$ (Materion, <45 μm), $MoTe_2$ (Materion, <10 μm), WS_2 (Sigma Aldrich, <2 μm), WSe_2 (Materion, <5 μm) and WTe_2 (American Elements). In all cases suspensions were prepared by adding 2.5 g of TMD powder to 50 ml of *N*-Methyl-2-pyrrolidone (NMP) from Sigma Aldrich in a glass beaker. Samples were sonicated using a stand mounted ultrasonic tip (Heilsher model UP200S, 200 W, 24 kHz) for 1.5 hours at 60% amplitude in pulsed mode with 1 s on 1 s off.

Following sonication, samples were transferred into glass vials and centrifuged at 5500 RPM for 2 hours in a Hettich Mikro 22R. A high RPM was chosen in order to remove the smallest flakes from these suspensions. This resulted in slightly coloured but light transparent supernatants with the majority of the material compacted at the bottom of the vial. At this point a solvent exchange was performed to facilitate working in a poorer, but easier to remove, low boiling point solvent. The supernatant was decanted and replaced with the same volume of HPLC grade isopropanol (IPA) before re-sonicating in a Branson 1510E-MT sonic bath (20 kHz) for 30 minutes. Following this, the samples were again centrifuged at 5500 RPM for a further two hours and the supernatant decanted once more. This step should remove a further portion of the smallest flakes as well as residual NMP likely left behind after the supernatant was first decanted. Samples were then topped up again with HPLC IPA and bath sonicated for a further 10 minutes to help homogenize the mixture.

The centrifugation regime chosen here ensures that our suspensions are mostly composed of larger flakes and partially exfoliated crystallites. Smaller flakes have a larger ratio of edge atoms to basal plane atoms. In our experience films made with smaller, better exfoliated flakes can exhibit negative photoconductivity effects on illumination, whereby the film becomes more resistive than in the dark.[38] These effects are known to occur in MoS_2 films[111] and will be studied in more detail in a future communication. Here our aim is to simply

compare the effect on the photoresponse of the films by varying the transition metal atom (M = Mo or W) and the chalcogen atom (X = S, Se or Te). As such, we opt for larger, less well exfoliated platelets to make our films.

These suspensions were used to form thin films for electrical testing. Films were formed using a method based in principle on the Langmuir–Blodgett method as described in our previous work.[37] Volumes of nanosheet-containing dispersion were deposited on the liquid–air interface such that a controlled nanosheet mass was deposited. This was adjusted such that roughly equal volumes of nanosheets were deposited and so the resulting film thickness would be ~1 μm in each case (assuming a film porosity of ~40%).[112] We accept that such a method can lead to some uncertainty in film thickness. However, we are confident the relative thickness error is <50% in each case. Once formed, films were transferred onto SiO_2/Si substrates (300 nm SiO_2) with lithographically pre-patterned, e-beam evaporated Ti–Au (5–45 nm) electrodes as illustrated in Fig. 1J. Once transferred, the films were allowed to dry in ambient conditions until all solvent had evaporated after a couple of minutes. At this point they were placed onto a hotplate at 200 °C for 3 minutes to promote adherence to the substrate and contacts. By repeating these steps one can build up thicker films if required. However, we note that the films can be very delicate making handling difficult. Here we perform the measurement with in plane geometry as opposed to the out of plane sandwich cell structure. The conductivity anisotropy is well known to be roughly three orders of magnitude for these layered materials.[37,113] A single coating (roughly 1 μm thick for each material) was used as there was no possibility of the electrodes shorting due to geometry. Silver paint and wire were used to connect the devices to a source meter. All electrical measurements were performed using a Keithley 2400 controlled by a LabView program.

It is worth noting that using gold as an electrode material for MTe_2 may be slightly problematic. For these materials, it was noted that, on checking the gold electrode's resistances before and after the mild 3 minute heating step (to promote film adherence to substrate and contacts, see above), the resistance had increased from ~150 Ω to ~175 Ω. No such increase in resistance was noted for MS_2 or MSe_2 based materials. It is well known that tellurium has a strong affinity for gold. This has been evidenced previously by us in heavily annealed $MoTe_2$ samples (not used in this study) on gold electrodes where the gold had been completely stripped away post-anneal, leaving only the titanium adhesion layer beneath. Thus, we believe care must be taken when using gold with Te-containing 2D materials.

Acknowledgements

We acknowledge the ERC for support *via* the project SEMANTICS. We would like to thank SFI for long-standing financial support and acknowledge additional funding from the Graphene Flagship (no. 604391).

References

1 V. Nicolosi, M. Chhowalla, M. G. Kanatzidis, M. S. Strano and J. N. Coleman, *Science*, 2013, **340**, 1226419.
2 A. K. Geim and I. V. Grigorieva, *Nature*, 2013, **499**, 419.
3 H. Li, J. Wu, Z. Yin and H. Zhang, *Acc. Chem. Res.*, 2014, **47**, 1067.
4 X. Huang, C. Tan, Z. Yin and H. Zhang, *Adv. Mater.*, 2014, **26**, 2185.
5 X. Huang, Z. Zeng and H. Zhang, *Chem. Soc. Rev.*, 2013, **42**, 1934.
6 M. Chhowalla, H. S. Shin, G. Eda, L.-J. Li, K. P. Loh and H. Zhang, *Nat. Chem.*, 2013, **5**, 263.
7 Q. H. Wang, K. Kalantar-Zadeh, A. Kis, J. N. Coleman and M. S. Strano, *Nat. Nanotechnol.*, 2012, **7**, 699.
8 J. A. Wilson and A. D. Yoffe, *Adv. Phys.*, 1969, **18**, 193.
9 K. S. Novoselov, D. Jiang, F. Schedin, T. J. Booth, V. V. Khotkevich, S. V. Morozov and A. K. Geim, *Proc. Natl. Acad. Sci. U. S. A.*, 2005, **102**, 10451.
10 A. Splendiani, L. Sun, Y. Zhang, T. Li, J. Kim, C.-Y. Chim, G. Galli and F. Wang, *Nano Lett.*, 2010, **10**, 1271.
11 K. F. Mak, C. Lee, J. Hone, J. Shan and T. F. Heinz, *Phys. Rev. Lett.*, 2010, **105**, 136805.
12 G. Eda, H. Yamaguchi, D. Voiry, T. Fujita, M. Chen and M. Chhowalla, *Nano Lett.*, 2011, **11**(12), 5111.
13 A. Kuc, N. Zibouche and T. Heine, *Phys. Rev. B: Condens. Matter*, 2011, **83**, 245213.
14 S. Tongay, J. Zhou, C. Ataca, K. Lo, T. S. Matthews, J. Li, J. C. Grossman and J. Wu, *Nano Lett.*, 2012, **12**(11), 5576.
15 P. Tonndorf, R. Schmidt, P. Böttger, X. Zhang, J. Börner, A. Liebig, M. Albrecht, C. Kloc, O. Gordan and D. R. T. Zahn, *Opt. Express*, 2013, **21**, 4908.
16 W. Zhao, Z. Ghorannevis, L. Chu, M. Toh, C. Kloc, P.-H. Tan and G. Eda, *ACS Nano*, 2013, **7**(1), 791.
17 J. Kang, S. Tongay, J. Zhou, J. Li and J. Wu, *Appl. Phys. Lett.*, 2013, **102**, 012111.
18 W. S. Yun, S. W. Han, S. C. Hong, I. G. Kim and J. D. Lee, *Phys. Rev. B: Condens. Matter*, 2012, **85**, 033305.
19 H. Jiang, *J. Phys. Chem. C*, 2012, **116**, 7664.
20 Y. Ma, Y. Dai, M. Guo, C. Niu, J. Lu and B. Huang, *Phys. Chem. Chem. Phys.*, 2011, **13**, 15546.
21 B. Radisavljevic, A. Radenovic, J. Brivio, V. Giacometti and A. Kis, *Nat. Nanotechnol.*, 2011, **6**, 147.
22 R. Gatensby, N. McEvoy, K. Lee, T. Hallam, N. C. Berner, E. Rezvani, S. Winters, M. O'Brien and G. S. Duesberg, *Appl. Surf. Sci.*, 2014, **297**, 139.
23 W. Zhang, J.-K. Huang, C.-H. Chen, Y.-H. Chang, Y.-J. Cheng and L.-J. Li, *Adv. Mater.*, 2013, **25**(25), 3456.
24 C. Yim, M. O'Brien, N. McEvoy, S. Riazimehr, H. Schafer-Eberwein, A. Bablich, R. Pawar, G. Iannaccone, C. Downing, G. Fiori, M. C. Lemme and G. S. Duesberg, *Sci. Rep.*, 2014, **4**, 5458.
25 N. Perea-López, A. L. Elías, A. Berkdemir, A. Castro-Beltran, H. R. Gutiérrez, S. Feng, R. Lv, T. Hayashi, F. López-Urías, S. Ghosh, B. Muchharla, S. Talapatra,

H. Terrones and M. Terrones, *Adv. Funct. Mater.*, 2013, **23**, 5511.
26 B. Radisavljevic, M. B. Whitwick and A. Kis, *ACS Nano*, 2011, **5**(12), 9934.
27 M. Shanmugam, C. A. Durcan and B. Yu, *Nanoscale*, 2012, **4**(23), 7399.
28 M. Shanmugam, T. Bansal, C. A. Durcan and B. Yu, *Appl. Phys. Lett.*, 2012, **101**, 263902.
29 V. Nicolosi, M. Chhowalla, M. G. Kanatzidis, M. S. Strano and J. N. Coleman, *Science*, 2013, **340**, 1420.
30 K. Chang and W. Chen, *Chem. Commun.*, 2011, **47**, 4252.
31 J.-Z. Wang, L. Lu, M. Lotya, J. N. Coleman, S.-L. Chou, H.-K. Liu, A. I. Minett and J. Chen, *Adv. Energy Mater.*, 2013, **3**, 798.
32 D. Hanlon, C. Backes, T. M. Higgins, M. Hughes, A. O'Neill, P. King, N. McEvoy, G. S. Duesberg, B. M. Sanchez, H. Pettersson, V. Nicolosi and J. N. Coleman, *Chem. Mater.*, 2014, **26**, 1751.
33 T. M. Higgins, D. McAteer, J. C. Mesquita Coelho, B. M. Sanchez, Z. Gholamvand, G. Moriarty, N. McEvoy, N. C. Berner, G. S. Duesberg, V. Nicolosi and J. N. Coleman, *ACS Nano*, 2014, **8**, 9567.
34 D. Voiry, M. Salehi, R. Silva, T. Fujita, M. Chen, T. Asefa, V. B. Shenoy, G. Eda and M. Chhowalla, *Nano Lett.*, 2013, **13**, 6222.
35 D. Voiry, H. Yamaguchi, J. Li, R. Silva, D. C. B. Alves, T. Fujita, M. Chen, T. Asefa, V. B. Shenoy, G. Eda and M. Chhowalla, *Nat. Mater.*, 2013, **12**, 850.
36 X. Huang, Z. Zeng, S. Bao, M. Wang, X. Qi, Z. Fan and H. Zhang, *Nat. Commun.*, 2013, **4**, 1444.
37 G. Cunningham, U. Khan, C. Backes, D. Hanlon, D. McCloskey, J. F. Donegan and J. N. Coleman, *J. Mater. Chem. C*, 2013, **1**(41), 6899.
38 D. Finn, M. Lotya, G. Cunningham, R. Smith, D. McCloskey, J. Donegan and J. N. Coleman, *J. Mater. Chem. C*, 2013, **2**(5), 925.
39 F. Withers, H. Yang, L. Britnell, A. P. Rooney, E. Lewis, A. Felten, C. R. Woods, V. Sanchez Romaguera, T. Georgiou, A. Eckmann, Y. J. Kim, S. G. Yeates, S. J. Haigh, A. K. Geim, K. S. Novoselov and C. Casiraghi, *Nano Lett.*, 2014, **14**, 3987.
40 F. Torrisi and J. N. Coleman, *Nat. Nanotechnol.*, 2014, **9**, 738.
41 N. Rouhi, D. Jain and P. J. Burke, *ACS Nano*, 2011, **5**, 8471.
42 G. Eda, G. Fanchini and M. Chhowalla, *Nat. Nanotechnol.*, 2008, **3**, 270.
43 K.-J. Baeg, M. Caironi and Y.-Y. Noh, *Adv. Mater.*, 2013, **25**, 4210.
44 K. R. Paton, E. Varrla, C. Backes, R. J. Smith, U. Khan, A. O'Neill, C. Boland, M. Lotya, O. M. Istrate, P. King, T. Higgins, S. Barwich, P. May, P. Puczkarski, I. Ahmed, M. Moebius, H. Pettersson, E. Long, J. Coelho, S. E. O'Brien, E. K. McGuire, B. M. Sanchez, G. S. Duesberg, N. McEvoy, T. J. Pennycook, C. Downing, A. Crossley, V. Nicolosi and J. N. Coleman, *Nat. Mater.*, 2014, **13**(6), 624.
45 G. Cunningham, M. Lotya, C. S. Cucinotta, S. Sanvito, S. D. Bergin, R. Menzel, M. S. P. Shaffer and J. N. Coleman, *ACS Nano*, 2012, **6**, 3468.
46 R. J. Smith, P. J. King, M. Lotya, C. Wirtz, U. Khan, S. De, A. O'Neill, G. S. Duesberg, J. C. Grunlan, G. Moriarty, J. Chen, J. Wang, A. I. Minett, V. Nicolosi and J. N. Coleman, *Adv. Mater.*, 2011, **23**, 3944.
47 C. Backes, R. J. Smith, N. McEvoy, N. C. Berner, D. McCloskey, H. C. Nerl, A. O'Neill, P. J. King, T. Higgins, D. Hanlon, N. Scheuschner, J. Maultzsch, L. Houben, G. S. Duesberg, J. F. Donegan, V. Nicolosi and J. N. Coleman, *Nat. Commun.*, 2014, **5**, 4576.
48 J. Li, M. M. Naiini, S. Vaziri, M. C. Lemme and M. Ostling, *Adv. Funct. Mater.*, 2014, **24**(41), 6524.
49 F. Torrisi, T. Hasan, W. Wu, Z. Sun, A. Lombardo, T. S. Kulmala, G.-W. Hsieh, S. Jung, F. Bonaccorso, P. J. Paul, D. Chu and A. C. Ferrari, *ACS Nano*, 2012, **6**, 2992.
50 Z. Yin, H. Li, H. Li, L. Jiang, Y. Shi, Y. Sun, G. Lu, Q. Zhang, X. Chen and H. Zhang, *ACS Nano*, 2012, **6**, 74.
51 O. Lopez-Sanchez, D. Lembke, M. Kayci, A. Radenovic and A. Kis, *Nat. Nanotechnol.*, 2013, **8**(7), 497.
52 D.-S. Tsai, K.-K. Liu, D.-H. Lien, M.-L. Tsai, C.-F. Kang, C.-A. Lin, L.-J. Li and J.-H. He, *ACS Nano*, 2013, **7**(5), 3905.
53 W. Choi, M. Y. Cho, A. Konar, J. H. Lee, G.-B. Cha, S. C. Hong, S. Kim, J. Kim, D. Jena, J. Joo and S. Kim, *Adv. Mater.*, 2012, **24**, 5832.
54 N. Perea-López, Z. Lin, N. R. Pradhan, A. Iñiguez-Rábago, A. L. Elías, A. McCreary, J. Lou, P. M. Ajayan, H. Terrones, L. Balicas and M. Terrones, *2D Materials*, 2014, **1**, 011004.
55 T. Dung-Sheng, L. Der-Hsien, T. Meng-Lin, S. Sheng-Han, C. Kuan-Ming, K. Jr-Jian, Y. Yueh-Chung, L. Lain-Jong and H. Hau Jr., *IEEE J. Sel. Top. Quantum Electron.*, 2014, **20**, 30.
56 H.-Y. Chang, S. Yang, J. Lee, L. Tao, W.-S. Hwang, D. Jena, N. Lu and D. Akinwande, *ACS Nano*, 2013, 130515142027004.
57 J. Pu, Y. Yomogida, K.-K. Liu, L.-J. Li, Y. Iwasa and T. Takenobu, *Nano Lett.*, 2012, **12**, 4013.
58 H. Tributsch, *Sol. Energy Mater.*, 1979, **1**, 257.
59 M. Bernardi, M. Palummo and J. C. Grossman, *Nano Lett.*, 2013, 130710144533003.
60 T. Löher, Y. Tomm, C. Pettenkofer, A. Klein and W. Jaegermann, *Semicond. Sci. Technol.*, 2000, **15**, 514.
61 M. Yamamoto, S. T. Wang, M. Ni, Y.-F. Lin, S.-L. Li, S. Aikawa, W.-B. Jian, K. Ueno, K. Wakabayashi and K. Tsukagoshi, *ACS Nano*, 2014, **8**(4), 3895.
62 A. Berkdemir, H. R. Gutiérrez, A. R. Botello-Méndez, N. Perea-López, A. L. Elías, C.-I. Chia, B. Wang, V. H. Crespi, F. López-Urías, J.-C. Charlier, H. Terrones and M. Terrones, *Sci. Rep.*, 2013, **3**, 1755.
63 B. C. Windom, W. G. Sawyer and D. W. Hahn, *Tribol. Lett.*, 2011, **42**, 301.
64 D. Lembke and A. Kis, *ACS Nano*, 2012, **6**, 10070.
65 S. Das, H.-Y. Chen, A. V. Penumatcha and J. Appenzeller, *Nano Lett.*, 2013, **13**, 100.

66 S. McDonnell, R. Addou, C. Buie, R. M. Wallace and C. L. Hinkle, *ACS Nano*, 2014, **8**, 2880.
67 R. H. Bube, *Photoconductivity of solids*, Wiley, 1960.
68 S. M. Sze, *Semiconductor Devices*, John Wiley and Sons, 1985.
69 W. Zhou, X. Zou, S. Najmaei, Z. Liu, Y. Shi, J. Kong, J. Lou, P. M. Ajayan, B. I. Yakobson and J.-C. Idrobo, *Nano Lett.*, 2013, **13**, 2615.
70 H.-P. Komsa, J. Kotakoski, S. Kurasch, O. Lehtinen, U. Kaiser and A. V. Krasheninnikov, *Phys. Rev. Lett.*, 2012, **109**(3), 035503.
71 D. Liu, Y. Guo, L. Fang and J. Robertson, *Appl. Phys. Lett.*, 2013, **103**, 18311.
72 K. Lee, H.-Y. Kim, M. Lotya, J. N. Coleman, G.-T. Kim and G. S. Duesberg, *Adv. Mater.*, 2011, **23**(36), 4178.
73 W. S. Hwang, M. Remskar, R. Yan, V. Protasenko, K. Tahy, S. D. Chae, P. Zhao, A. Konar, H. Xing, A. Seabaugh and D. Jena, *Appl. Phys. Lett.*, 2012, **101**, 013107.
74 W. Liu, J. Kang, D. Sarkar, Y. Khatami, D. Jena and K. Banerjee, *Nano Lett.*, 2013, **13**, 1983.
75 H. Fang, S. Chuang, T. C. Chang, K. Takei, T. Takahashi and A. Javey, *Nano Lett.*, 2012, **12**, 3788.
76 S. Das and J. Appenzeller, *Appl. Phys. Lett.*, 2013, **103**, 103501.
77 P. D. Antunez, D. H. Webber and R. L. Brutchey, *Chem. Mater.*, 2013, **25**, 2385.
78 S. Larentis, B. Fallahazad and E. Tutuc, *Appl. Phys. Lett.*, 2012, **101**, 223104.
79 B. Chamlagain, Q. Li, N. J. Ghimire, H.-J. Chuang, M. M. Perera, H. Tu, Y. Xu, M. Pan, D. Xaio, J. Yan, D. Mandrus and Z. Zhou, *ACS Nano*, 2014, 140416143016002.
80 S. Fathipour, *IEEE*, 2013, 115.
81 X. Yu, M. S. Prévot and K. Sivula, *Chem. Mater.*, 2014, **26**, 5892.
82 G. Cunningham, M. Lotya, N. McEvoy, G. S. Duesberg, P. van der Schoot and J. N. Coleman, *Nanoscale*, 2012, **4**(20), 6260.
83 N. Mazumdar, R. Sarma, B. K. Sarma and H. L. Das, *Bull. Mater. Sci.*, 2006, **29**, 11.
84 R. H. Bube, *Photoelectronic Properties of Semiconductors*, Cambridge University Press, 1992.
85 L. L. Kazmerski, *Polycrystalline and amorphous thin films and devices*, Academic Press, 1980.
86 H. C. Card and E. S. Yang, *Electron. Devices, IEEE Trans. Electron. Devices*, 1977, **24**, 397.
87 A. V. Sukach, V. V. Tetyorkin and N. M. Krolevec, *Semicond. Phys., Quantum Electron. Optoelectron.*, 2010, **13**, 221.
88 A. Rose, *Concepts in photoconductivity and allied problems*, Interscience Publishers, 1963.
89 A. S. Maan and D. R. Goyal, *Optoelectron. Adv. Mater.*, 2007, **1**, 430.
90 V. Halpern, *J. Phys. C: Solid State Phys.*, 1988, **21**, 2555.
91 R. K. Pal, S. Yadav, A. K. Agnihotri, D. Kumar and A. Kumar, *J. Non-Oxide Glasses*, 2009, **1**, 285.
92 K. Dolui, I. Rungger, C. D. Pemmaraju and S. Sanvito, *Phys. Rev. B: Condens. Matter*, 2013, **88**(7), 075420.
93 K. Dolui, I. Rungger and S. Sanvito, *Phys. Rev. B: Condens. Matter*, 2013, **87**(16), 165402.
94 A. Ayari, E. Cobas, O. Ogundadegbe and M. S. Fuhrer, *J. Appl. Phys.*, 2007, **101**, 014507.
95 W. Gu, J. Shen and X. Ma, *Nanoscale Res. Lett.*, 2014, **9**, 1.
96 N. R. Pradhan, D. Rhodes, Q. Zhang, S. Talapatra, M. Terrones, P. M. Ajayan and L. Balicas, *Appl. Phys. Lett.*, 2013, **102**, 123105.
97 S. Kim, A. Konar, W.-S. Hwang, J. H. Lee, J. Lee, J. Yang, C. Jung, H. Kim, J.-B. Yoo, J.-Y. Choi, Y. W. Jin, S. Y. Lee, D. Jena, W. Choi and K. Kim, *Nat. Commun.*, 2012, **3**, 1011.
98 S. Ghatak, A. N. Pal and A. Ghosh, *ACS Nano*, 2011, **5**, 7707.
99 C. Ballif, M. Regula, F. Lévy, F. Burmeister, C. Schafle, T. Matthes, P. Leiderer, P. Niedermann, W. Gutmannsbauer and R. Bucher, *J. Vacuum Sci. Technol. A*, 1998, **16**, 1239.
100 C. Maurel, F. Ajustron, R. Péchou, G. Seine and R. Coratger, *Surf. Sci.*, 2006, **600**, 442.
101 Z. Zeng, Z. Yin, X. Huang, H. Li, Q. He, G. Lu, F. Boey and H. Zhang, *Angew. Chem., Int. Ed.*, 2011, **50**, 11093.
102 M. Fontana, T. Deppe, A. K. Boyd, M. Rinzan, A. Y. Liu, M. Paranjape and P. Barbara, *Sci. Rep.*, 2013, **3**, 1634.
103 S. H. El-Mahalawy and B. L. Evans, *Phys. Status Solidi B*, 1977, **79**, 713.
104 S. R. Thakurta and A. K. Dutta, *J. Phys. Chem. Solids*, 1983, **44**, 407.
105 S. M. Sze and K. K. Ng, *Physics of Semiconductor Devices*, Wiley, 2006.
106 C. Kittel, *Introduction to solid state physics*, Wiley, Hoboken, NJ, 2005.
107 B. Choubey, D. Joseph, S. Aoyama and S. Collins, in 30th International Congress of Imaging Science, 2006.
108 S. Ghanbarzadeh, S. Abbaszadeh and K. S. Karim, *IEEE Electron. Device Lett.*, 2014, **35**, 235.
109 M. R. Esmaeili-Rad and S. Salahuddin, *Sci. Rep.*, 2013, **3**, 2345.
110 M. Makarova, Y. Okawa and M. Aono, *J. Phys. Chem. C*, 2012, **116**, 22411.
111 A. Serpi, *Phys. Status Solidi A*, 1992, **133**, 73.
112 U. Khan, A. O'Neill, M. Lotya, S. De and J. N. Coleman, *Small*, 2010, **6**, 864.
113 X. Tian, M. E. Itkis, E. B. Bekyarova and R. C. Haddon, *Sci. Rep.*, 2013, **3**, 1710.

